Shape Modulation of Tungstic Acid and Tungsten Oxide Hollow Structures

ARTICLE *in* THE JOURNAL OF PHYSICAL CHEMISTRY C · APRIL 2009

Impact Factor: 4.77 · DOI: 10.1021/jp900160u

2 AUTHORS, INCLUDING:

Masahiro Miyauchi
Tokyo Institute of Technology
96 PUBLICATIONS **3,541** CITATIONS

THE JOURNAL OF PHYSICAL CHEMISTRY C

Article

Shape Modulation of Tungstic Acid and Tungsten Oxide Hollow Structures

Zhi-Gang Zhao, and Masahiro Miyauchi

J. Phys. Chem. C, **2009**, 113 (16), 6539-6546• Publication Date (Web): 30 March 2009

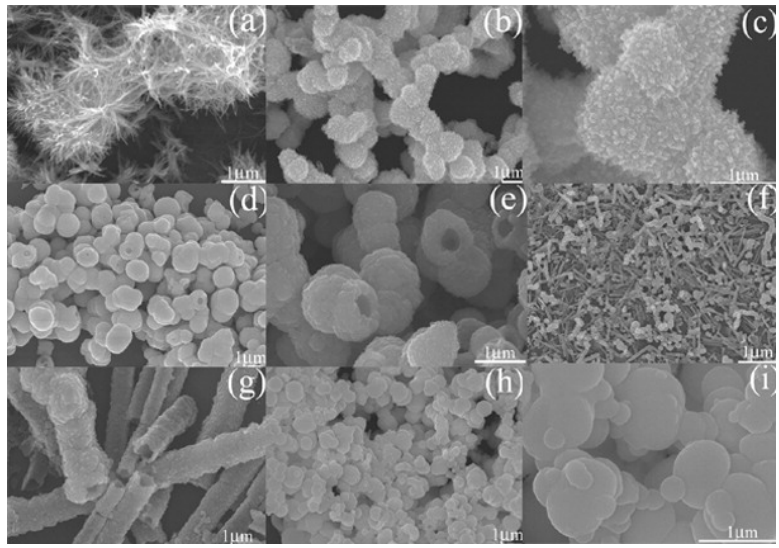

More About This Article

Additional resources and features associated with this article are available within the HTML version:

- Supporting Information
- Access to high resolution figures
- Links to articles and content related to this article
- Copyright permission to reproduce figures and/or text from this article

View the Full Text HTML

Shape Modulation of Tungstic Acid and Tungsten Oxide Hollow Structures

Zhi-Gang Zhao and Masahiro Miyauchi*

Nanotechnology Research Institute, National Institute of Advanced Industrial Science and Technology, Tsukuba Central 5, 1-1-1 Higashi, Tsukuba, Ibaraki 305-8565, Japan

Received: January 07, 2009; Revised Manuscript Received: March 06, 2009

Tungstic acid ($H_2W_{1.5}O_{5.5}\cdot H_2O$) hollow structures, including hollow spheres, nanotubes, and hollow boxes, have been selectively synthesized by a nonaqueous and surfactant-free solvothermal method. The synthesis involves the alcoholeysis of WCl_6 in the presence of urea. A series of experimental factors such as the urea amount, ethanol amount, reaction temperature, reaction time, and pH value have important influences on the morphology and size of the products on the basis of scanning electronic microscopy and X-ray powder diffraction characterizations. The subsequent slow annealing leads to the formation of tungsten oxide (WO_3), the hollow morphology of which is well-retained. The most striking feature of these WO_3 hollow structures is the resultant nanoporous walls or shells, which may lead to potential applications in many fields, including energy storage, catalysis, and biotechnology.

Introduction

The surge of interest in carbon nanotubes has led scientists to search for other inorganic hollow micro- and nanostructures having tailored structures, low densities, and high surface areas because they have potential applications across various technological fields as photonic crystals, drug-delivery carriers, and sensors and can be used in catalysis or chemical reactors.[1−4] So far, the synthetic strategies for inorganic hollow structures include well-established approaches such as conventional hard-templating (silica spheres, polystyrene beads, carbon nanoparticles, and so on) and soft-templating methods (emulsion droplets, supramolecular micelles, gas bubbles, and so on) as well as newly emerging methods based on sacrificial templating and template-free synthesis.[5] These methods have been extensively applied to prepare hollow structures from a wide range of inorganic materials, including TiO_2,[6] SnO_2,[7] Fe_3O_4,[8] ZnS,[9] Pt,[10] and others. However, most as-prepared hollow structures are of spherical shape, and the synthesis of nonspherical hollow structures remains a significant challenge.

Tungsten oxide (WO_3) has many potential applications in broad areas of electrochromic windows, nonemissive displays, information storage media, photonic crystals, optical devices, gas sensors, and photocatalysts.[11] Because WO_3 nanomaterials exhibit superior properties in some promising applications compared with those of bulk materials, much effort has been contributed to WO_3 nanostructures (nanowires, nanotubes, nanobelts, and nanoplatelets).[12−18] Although WO_3 hollow spheres were synthesized by controlled hydrolysis of WCl_6 employing novel carbon microspheres as templates,[19] the synthesis of WO_3 hollow structures is still rather rare, especially by the template-free solvothermal method. A series of three dimensional (3D) WO_3 hollow structures, including hollow dendrites, spheres, and dumbbells, were realized by calcining the acid-treated $PbWO_4$ and $SrWO_4$ at 500 °C for 2 h.[20] However, it still remains a great challenge to synthesize WO_3 hollow structures under mild solvothermal conditions. Recently, a new surfactant-free nonaqueous synthetic strategy, involving only metal oxide precursors and common organic solvents, has emerged as one of the most versatile and powerful synthesis methodologies for metal oxide nanomaterials.[21] In our previous study, we modified this strategy by adding urea as a ligand in organic solvents and prepared tungstic acid nanotubes through a solvothermal reaction in a WCl_6/urea/ethanol system and nanoporous-walled WO_3 nanotubes after subsequent slow calcinations.[22] However, systematic knowledge about morphology control, determining factors, and dynamic processes in the reaction system is still lacking, and more mechanism studies are required to understand this intriguing process.

In this paper, we report how a WCl_6/urea/ethanol system can be controlled to produce tungstic acid hollow spheres, nanotubes, and even hollow boxes and show how the shape of tungstic acid hollow structures evolves by systematically varying the urea amount, ethanol amount, and reaction time. The influence of factors such as the pH value, temperature, and order of precursor addition was also described. The findings imply that a complex dissolution−precipitation mechanism is likely to be responsible for the production of hollow spheres and suggest that the novel growth of the nanotubes occurred via oriented attachment of hollow spheres assisted by a one-dimensional urea hydrogen-bonded chain. Upon slow annealing, WO_3 hollow structures with the same shape could be obtained, and the most striking feature is the resultant nanoporous walls or shells. Gas-phase acetaldehyde decomposition was used as a probe reaction to evaluate the photocatalysis of Pt-loaded WO_3 nanotubes, hollow spheres, and solid spheres under visible light illumination.

Experimental Procedures

Preparation of Tungstic Acid Hollow Structures. In a typical synthesis, WCl_6 (0.397 g, 1 mmol) and a certain amount of urea were added to 40 mL of absolute ethanol, and the mixture was loaded into a Teflon-lined autoclave. The autoclave was sealed and transferred into an oven that was maintained at 180 °C for 12 h. After cooling to room temperature naturally, white precipitate was collected and rinsed several times with distilled water and absolute ethanol before being dried at 60 °C for 12 h.

* To whom correspondence should be addressed: E-mail: m-miyauchi@aist.go.jp.

10.1021/jp900160u CCC: $40.75
Published on Web 03/30/2009

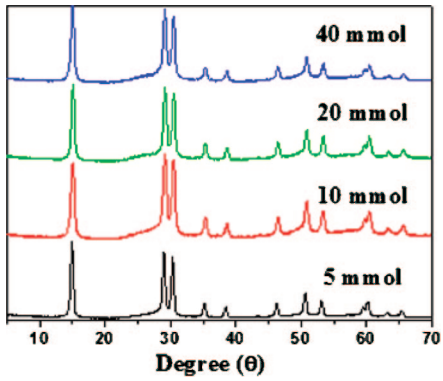

Figure 1. XRD pattern of the as-prepared samples with urea additions of (a) 5 mmol, (b) 10 mmol, (c) 20 mmol, and (d) 40 mmol.

Preparation of WO_3 Hollow Structures. Tungstic acid samples were transformed to WO_3 through subsequent annealing. To retain the original structure, tungstic acid hydrate samples were slowly heated from room temperature to 450 °C in 3 h and annealed at 450 °C for another 3 h to obtain the final yellow products.

Characterization. A Hitachi S-4800 field emission scanning electron microscope (FESEM, Hitachi Co., Ltd. S-4800) was used to investigate the morphology. Transmission electron microscope (TEM) images were collected by using a JEOL JEM 2010F microscope working at 100 kV. X-ray powder diffraction (XRD, Rigaku Co., Ltd. Ultima-X) measurements were carried out using filtered Cu Kα radiation. The nitrogen adsorption and desorption isotherms at 77 K were measured using a Micrometrics ASAP 2010 system after the samples were degassed in vacuum at 90 °C overnight, while the Barrett−Joyner−Halenda (BJH) method was used to calculate the average pore diameter.[23]

Photocatalytic Activity Measurement. The samples were illuminated with a 150 W Xe lamp (Hayashi Watch-Works Co., Ltd.). The catalysts (100 mg) were placed in a circular glass dish and mounted in the reactor. Then a certain amount of gas-phase acetaldehyde was introduced into the reactor by syringe until the concentration of acetaldehyde in the reactor reached about 500 ppmv. Before analysis, the catalyst and acetaldehyde were kept in the dark for 1 h to ensure the establishment of an adsorption−desorption equilibrium between the photocatalyst and acetaldehyde. The acetaldehyde and CO_2 concentrations were measured using a gas chromatograph (Shimadzu model GC-2014) equipped with a 2 m Porapak-Q column, a methanizer, and a flame ionization detector, using N_2 as the carrier gas.

Results and Discussion

Synthesis. With the aim of obtaining a clear understanding of the crystal growth in the WCl_6/urea/ethanol system, we varied the urea amount, ethanol amount, reaction temperature, reaction time, pH value, and so on.

Urea Amount. To validate the role of urea, a series of contrast experiments with different amounts of urea were conducted under the same reaction conditions. All peaks in XRD patterns of all samples (Figure 1) could be indexed as pure tungstic acid hydrate, $H_2W_{1.5}O_{5.5}\cdot H_2O$ (space group: $Fd\bar{3}m$ (No. 227)) with lattice constants $\alpha = \beta = \gamma = 10.214$ Å (JCPDS 48-0719). The strong and sharp diffraction peaks indicated that the products were well crystallized.

Although the yielded crystalline phases with urea addition are the same, the morphologies have drastic differences relative to the amount of urea on the basis of SEM and TEM images. When pure WCl_6 was used and no urea was introduced during the synthesis, the products adopted an urchin-like appearance, consisting of numerous one-dimensional nanowires of high density pointing toward the center (Figure 2a). When 5 mmol of urea was added to the reaction solutions, interconnected spheres with a shaggy appearance could be distinguished in the samples (Figure 2b). A close examination of one sphere (Figure 2c) showed that the sphere's surface was not smooth and was covered by small nanoparticles. When the urea amount was increased to 10 mmol, the product consisted entirely of well-defined discrete bowl-like hollow spheres with diameters in the range of 1−5 μm and wall thicknesses of 200−500 nm (Figure 2d,e). TEM was used to further confirm the hollow nature of the spheres (inset, Figure 2e), and a strong contrast between the dark edge and pale center could be seen. These results indicated that the addition of urea facilitated the formation of hollow structures and improved the monodispersity, similar to a recent report that urea was used for the formation of well-dispersed SnO_2 hollow nanospheres with good monodispersity.[24] When the urea amount was further increased to 20 mmol, the samples were usually crystallized into an interesting tubular nanostructure. As shown in panels f and g of Figure 2, the product was composed of a large quantity of well-dispersed nanotubes that were open on both ends and had outer diameters of approximately 300−1000 nm and lengths of 5−20 μm. Hollow structures were not further observed and solid egg-shaped nanoparticles appeared instead when the urea amount was too high, e.g., above 40 mmol. These nanoparticles had fairly smooth surfaces, and the particle size was in the range of 300−1000 nm (Figure 2h,i). Therefore, neither extremely low nor high amounts of urea were suitable for the construction of hollow nanostructures.

Interestingly, while the majority of the particles were generally spherical at the urea amount of 5 mmol, a small fraction of the particles had a cubic shape with a hollow core in the product as confirmed by SEM (Figure 3a,b). The sizes of the hollow boxes were about 1−10 μm. Compared to their spherical counterparts, the synthesis of hollow particles with well-defined cubic shapes is a significant challenge to materials scientists.[5] To the best of our knowledge, this is the first time a box-like hollow structure for WO_3 has been observed. The two types of morphology obtained in the same reaction system imply two distinct mechanisms of nucleation and growth of the nanocrystals for hollow boxes and spherical particles. Homogenous nucleation and aggregation growth are considered to take place in the absence of any capping agent. Urea can act as a capping agent to modify the crystal structure of tungstic acid when precipitated by alcohol in the presence of urea,[25] but possibly it only partially blocks the crystal growth when the urea concentration is low at 5 mmol. Therefore, homogeneous nucleation and aggregation growth are still the dominant growth mechanism. Thus, most of the products, in turn, were spherical particles in a typical synthesis with a minor amount of hollow boxes.

Reaction Time. During the course of examinations, reaction time was varied. We systematically investigated the effect of the synthesis period from 2 to 12 h with the addition amount of urea and ethanol fixed at 20 mmol and 40 mL, respectively. XRD patterns indicated that all of the time-series samples were tungstic acid hydrate, $H_2W_{1.5}O_{5.5}\cdot H_2O$. The morphologies of the resultant products in different stages of 2, 4, 8, and 12 h are presented in Figure 4a−h, respectively. At the first stage (2 h), hollow spheres with a diameter of 1−5 μm and a thickness of ∼100 nm were observed (Figure 4a). More importantly, the

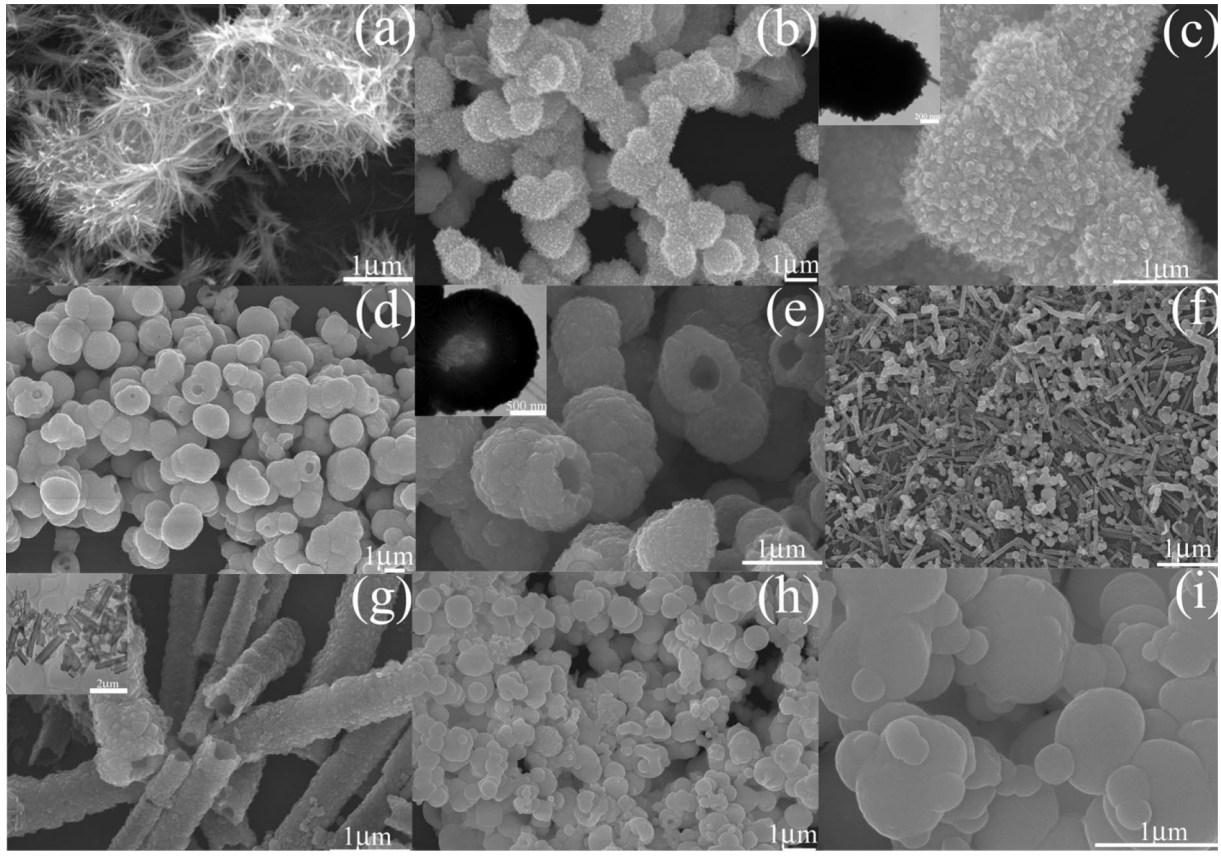

Figure 2. SEM and TEM (inset) images of the as-prepared samples with urea additions of (a) 0 mmol, (b,c) 5mmol, (d,e) 10 mmol, (f,g) 20 mmol, and (h,i) 40 mmol.

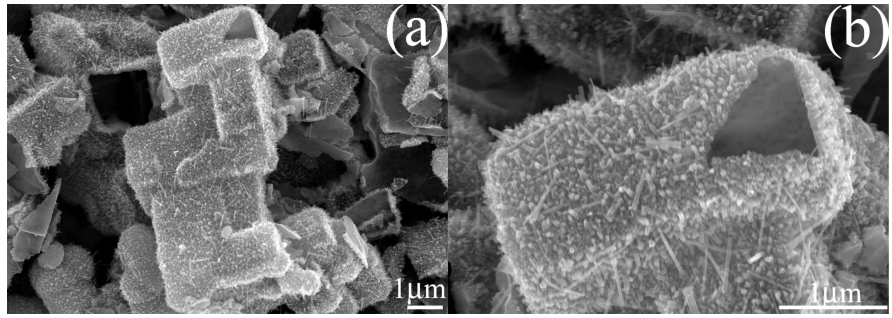

Figure 3. SEM images of the as-prepared hollow boxes at the urea addition of 5 mmol.

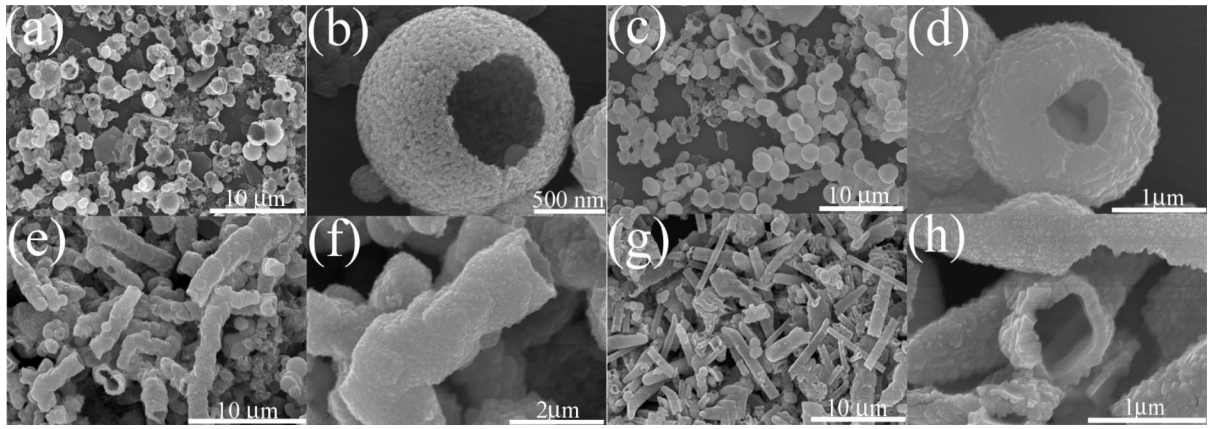

Figure 4. SEM images of the as-prepared samples with reaction times of (a,b) 2 h, (c,d) 4 h, (e,f) 8 h, and (g,h) 12 h.

hollow spheres were loosely assembled from many particles of decades of nanometers, as shown in an enlarged view (Figure 4b). Increase in the reaction time to 4 h produced similar hollow spheres with an outer diameter still in the range of 1−5 μm (Figure 4c). However, as revealed in Figure 4d, there was a high degree of agglomeration and coalition between nanopar-

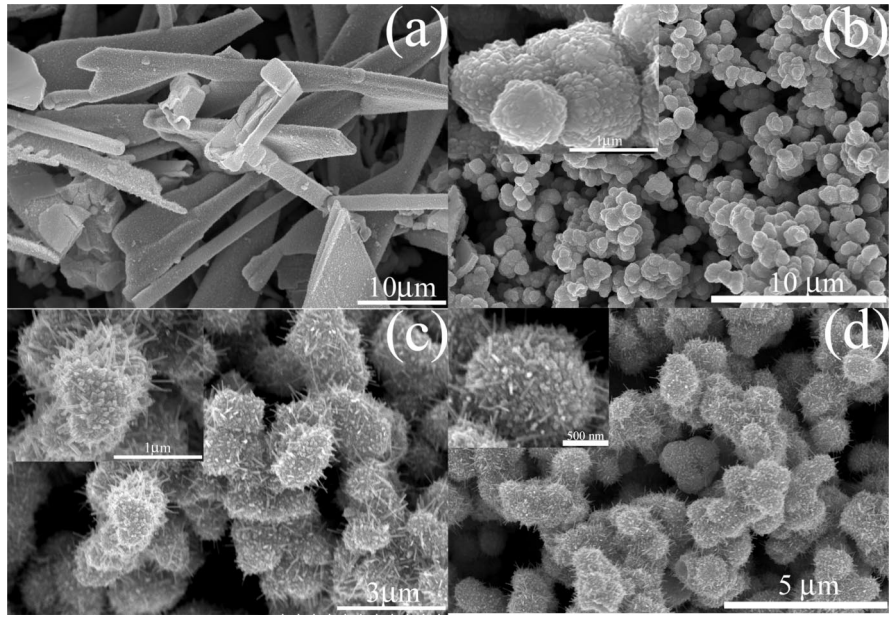

Figure 5. SEM images of the as-prepared samples with ethanol additions of (a) 10 mL, (b) 20 mL, (c) 45 mL, and (d) 60 mL.

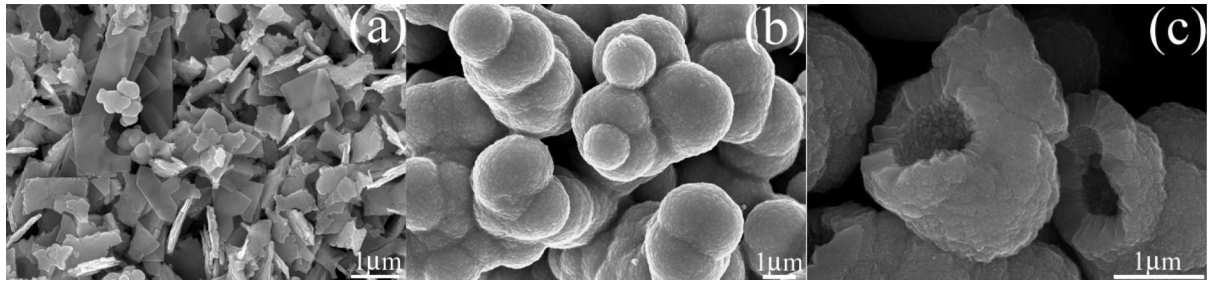

Figure 6. SEM images of the as-prepared samples with reaction temperatures of (a) 100 °C, (b) 140 °C, and (c) 180 °C.

ticles on the shell, possibly through the Ostwald ripening mechanism, in which the larger crystals grow at the expense of the small crystals.[24] Also, the dimension of the cavity is relatively small compared to the volume of those spheres with the reaction time of 2 h. When the synthesis time was prolonged to 8 h, a drastic change in morphology was observed. The samples consisted mostly of curved nanotubes (Figure 4e), although a minor amount of hollow spheres were still occasionally seen. The tubes were typically less than 1000 nm in diameter and in the range of 5−20 μm in length. One thing we should notice is that most of the nanotubes were divided into several segments and showed a bamboo-like shape, which is discussed later. The total conversion of hollow spheres into nanotubes took approximately 12 h (Figure 4g,h). The SEM images clearly display the straight tube structure of tungstic acid and the size in lateral dimensions with widths of about 300−1000 nm. These nanotubes were open on two ends and had solid walls with a considerably uniform thickness of about 100 nm. The cross-section was of a nearly rectangular width of ~250 nm.

Ethanol Amount. The relative amounts of ethanol were also adjusted. The amount of WCl_6 and urea were fixed at 1 and 5 mmol, respectively, with the ethanol amount systematically changing from 10 to 60 mL. When the amount of ethanol was 10 mL in the solution, a carpet-like structure was the predominant product (Figure 5a), and the product surfaces were quite rough, possibly because of a self-assembly mechanism in which small nanoparticles congregate into a carpet-like structure. When the ethanol amount was altered to 20 mL, while other parameters were kept constant, spherical particles with diameters ranging from 1 to 5 μm were observed (Figure 5b). The spheres were comprised of much smaller nanoparticles, similar to a quite common phenomenon in self-assembly processes. When the ethanol amount was increased to 50 mL, the surfaces of the spheres became more prickly. Some short nanorods with diameters ranging from 40−50 nm protruded from the surface of the spherical particles and formed urchin-like fuzzy shapes composed of spheres as the cores and nanorods as the shells (Figure 5c). When the ethanol amount was increased to 60 mL, more nanorods appeared on the surface of spherical particles (Figure 5d). It can be envisioned that the larger ethanol amount, the smaller the relative precursor concentration. Accordingly, the spheres as the cores will shrink further, and the nanorods as the shells will lengthen further. The ultimate condition is very close to that as in the absence of urea, which is an urchin-like pattern totally assembled by nanowires.

Reaction Temperature, pH Value, and Order of the Precursor Addition. Reaction temperature is a vital factor for morphology (Figure 6a−c). With a constant urea amount of 10 mmol and an ethanol amount of 40 mL, the product consisted entirely of discrete bowl-like hollow spheres (Figure 6c) at 180 °C, whereas solid spheres were formed, as displayed in Figure 6b, when the reaction temperature was decreased down to 140 °C. Comparatively, the products prepared at the temperature of 100 °C usually were flake-like structures (Figure 6a).

Further experiments demonstrated that the pH value in the reactant solutions has an important influence on the morphologies of the products. The different pH values were controlled by NaOH or HCl drops. Without the addition of NaOH or HCl, the optimal pH value for the synthesis of tubular structures was

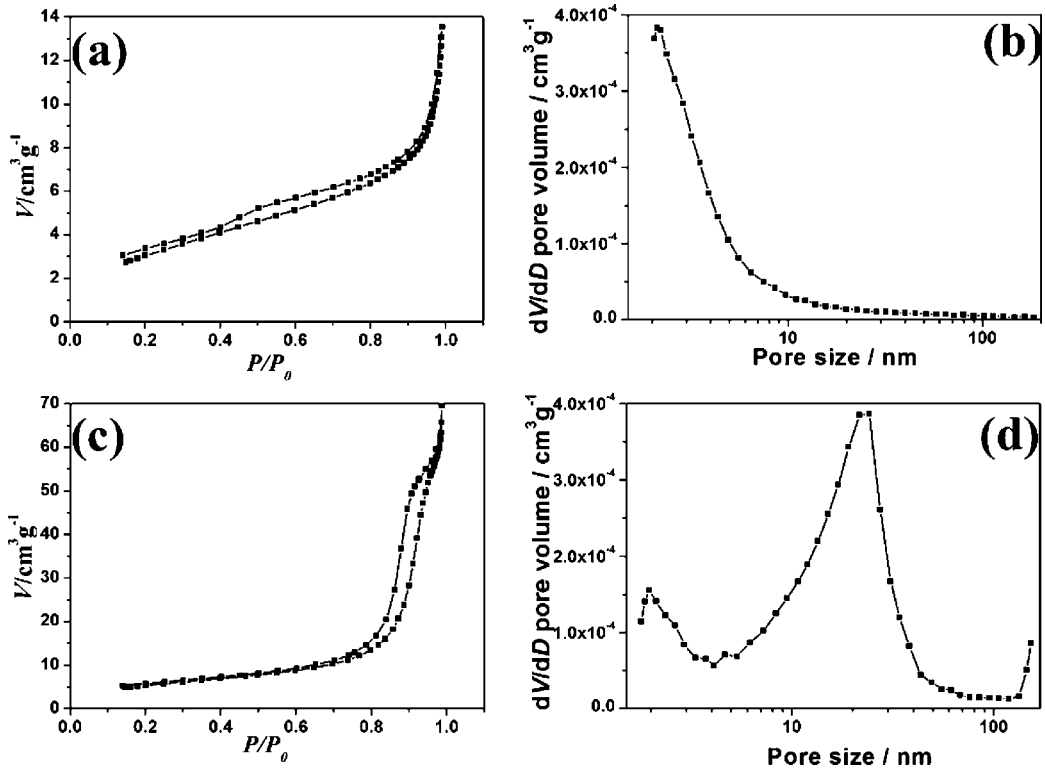

Figure 7. Nitrogen adsorption−desorption isotherm plot of tungstic acid (a) and tungsten oxide (c) hollow spheres, and Barrett−Joyner−Halenda (BJH) pore size distribution plot of tungstic acid (b) and tungsten oxide (d) hollow spheres.

about 5−6. When the pH value was increased to 12 or decreased to 1, the products had no specific shape, and no micro- or nanostructures were formed. These results indicate that the morphologies of the final products were sensitive to pH values in the precursor solution. Furthermore, we studied how the addition order of urea and WCl_6 in ethanol affected morphology. It was found that the order of ingredient addition had little influence on morphology.

Nanoporous-Walled Feature of WO_3 Hollow Structures after Annealing. Upon slow annealing, WO_3 hollow structures were obtained with the shape maintained. However, pores were formed at sidewalls, and possessing nanoporous walls or shells is the most striking feature for these WO_3 hollow structures, which provides active sites for cocatalyst particles in photocatalysis. Our previous studies have revealed that WO_3 nanotubes with mesopores and macropores in the walls exhibited superior photocatalytic ability.[22] The isotherms of nitrogen and adsorption at 77 K for hollow spheres prepared by solvothermal process followed by calcinations at 450 °C for 3 h are plotted in Figure 7. The isotherms of hollow spheres before and after calcinations can be categorized as type III, with distinct hysteresis loops observed in the range of 0.40−0.80 P/P_0 (Figure 7a) and 0.80−0.96 P/P_0 (Figure 7b), respectively. From the isotherms, the BET surface area of the sample before and after calcinations can be calculated to be 12.2 and 24.0 m^2g^{-1}, respectively. The pore size distribution of the sample before and after calcinations is also given in panels b and d of Figure 7. It can be seen that the sample after calcinations predominantly contained pores in the range of 5−60 nm (mesopores and macropores), which can be attributed to its porous sidewalls.

Formation Mechanism of Tungstic Acid Hollow Structures. In the study by Choi et al., only monoclinic $W_{18}O_{49}$ nanorods were synthesized in a WCl_6/ethanol system.[12] Whereas our results strongly supported that the solution chemistry for this system in the solvothermal synthesis is greatly affected by urea, and various controlled hollow structures can be obtained. The overall results on the products under different reaction conditions, using WCl_6 and urea as the starting materials, are briefly summarized in Table 1.

On the basis of these experimental results, the possible growth process of hollow structures can be proposed (Figure 8). WCl_6 first dissolves in ethanol to form a 6-fold coordinated $[WCl_m(OC_2H_5)_{6-m}]^{2-}$ complex species and HCl, similar to the case of $TiCl_4$ reported by Wang et al.[26] The complex species can serve as a barrier against the hydrolysis of WCl_6 with residual water; thus, a solution without precipitates can be obtained before the solvothermal process. The linking between the complex species is carried out to form WO_3 by a condensation reaction in the solvothermal process, but a large amount of Cl^- coming from the alcoholeysis of WCl_6 can retard this condensation reaction.

On the other hand, it was recently reported that urea can be used in organic crystal assembly from one-dimensional chains to nanotubes because of its strong hydrogen-bonding group.[27] We believe that urea also plays an important role in the formation of hollow structures in our study. When urea is added into the solution as a capping agent, urea molecules having amino groups with a high electronegativity can chelate to the W ions. As the urea content is increased, the chelation also became stronger. In the initial period, a large amount of small $[WCl_m(OC_2H_5)_{6-m}]^{2-}$ clusters aggregate to form solid spheres due to homogeneous nucleation and aggregation growth (Figure 8A). The spherical aggregates are indispensable to the formation of hollow spheres. Strong acid or basic conditions, which are far from the isoelectric point, are not appropriate to form hollow structures on the basis of the pH dependence of the aggregate morphology described above. Recently, Li et al. reported the synthesis of photocatalytic hollow titania spheres with tunable interior structures transiting from dense to sphere-in-sphere to hollow, and the process followed a dissolution−reprecipitation

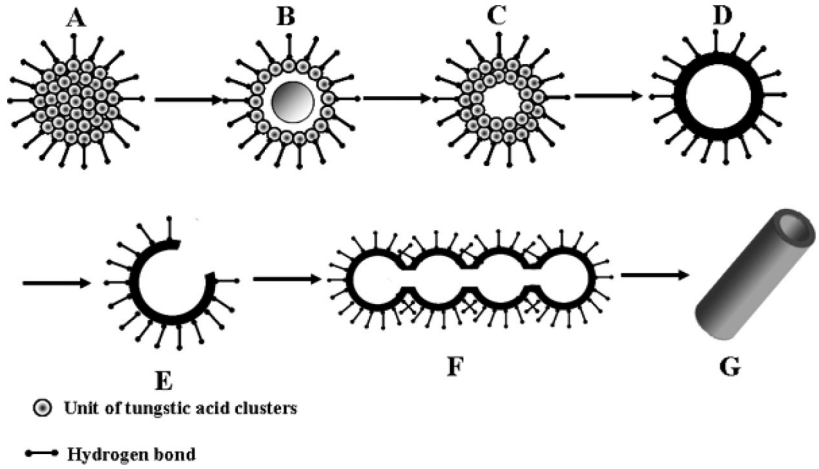

Figure 8. Schematic diagram of the proposed formation mechanism of tungstic acid hollow spheres and nanotubes.

TABLE 1: Summary of the Products Obtained under Different Reaction Conditions

reaction temperature (°C)	reaction time (hours)	urea amount (mmol)	ethanol amount (ml)	morphology of the main product
180	12	0	40	nanowires
180	12	5	40	interconnected solid spheres
180	12	10	40	discrete hollow spheres
180	12	20	40	nanotubes
180	12	40	40	egg-shaped particles
180	2	20	40	hollow spheres
180	4	20	40	hollow spheres
180	8	20	40	curved nanotubes
180	12	20	40	nanotubes
180	12	5	10	carpet-like
180	12	5	20	interconnected solid spheres
180	12	5	50	urchin-like solid spheres
180	12	5	60	urchin-like solid spheres
100	12	10	40	flake-like
140	12	10	40	solid spheres
180	12	10	40	hollow spheres

mechanism.[28] It can be seen that a sphere−sphere structure is an intermediate in the morphology evolution from a solid sphere to a totally hollow structure. With a prolonged reaction time, a similar hollow effect is expected to appear in our synthesis. HCl in the solution dissolves the surface-building clusters of the solid spheres and redeposits from the solution to grow into a thin layer (Figure 8B). Continuation of this process gradually dissolves the core spheres, which could induce the transference of a chemical substance from inside to outside, and constructs the observed hollow spheres (Figure 8C). Then adjacent nanocrystals in the shell layer of the hollow spheres fuse together (Figure 8D). The fresh prepared hollow spheres have closed shells, but the shells can be broken by HCl from the alcoholeysis and/or thermally induced stress (Figure 8E). With a further increase in reaction time, the urea molecule specifically adsorbs onto sphere interfaces and guides the oriented attachment of hollow spheres, eventually resulting in the formation of nanotubes with rough surfaces. This hypothesis is based on the fact that urea molecules can form one-dimensional hydrogen-bonded chains by employing their two NH proton donors, and the C═O protons acceptor in bifurcated hydrogen bonds at a certain concentration.[27] Assisted by the strong and directional urea hydrogen-bonded chains in a WCl_6/urea/ethanol system, the adsorbed urea molecules assemble the single hollow spheres into one-dimensional hollow bead chain-like structures (Figure 8F). In the final stage, because higher reactivity is expected for these interfaces between the interconnected hollow spheres, the interfaces with high reactivity usually diminish rapidly during the crystal growth process as a result of the minimization of surface energy. Finally solid and straight walls with smooth surface in nanotubes are formed by promoting Ostwald ripening within the walls (Figure 8G).

Supporting evidence for the growth mechanism was uncovered by the observation of some interesting morphology in the products. Figure 9a shows a unique sphere-in-sphere structure with a size of about 1000 nm. Because a sphere-in-sphere structure is an intermediate in the growth mechanism proposed by Li et al., its observation indicates that the formation mechanism of tungstic acid hollow spheres is also dominated by the dissolution−reprecipitation mechanism.[28] Figure 9b shows a SEM image of an isolated and curved nanotube at a synthesis time of 8 h, which is obviously comprised of several hollow spheres. Because Ostwald ripening has not yet finished within the walls, this nanotube possesses a bead-like periodic structure. The diameter of the nanotube periodically changes, and the distance between knots is almost uniform, which is comparable to the diameter of hollow spheres. The existence of a bead-like structure confirms that the formation of nanotubes occurred via oriented attachment of hollow spheres.

It is noticeable that the formation of nanotubes can only occur in a certain range of urea amount and needs adequate reaction time. This might result from the fact that the assembly from hollow spheres to nanotubes needs a comparatively stronger chelation force as well as more urea. However, excessive urea loading results in failure of the formation of hollow structures. A large amount of OH^- ions released from the decomposition of urea decrease the solution acidity and speed up the condensation reaction. At this condition, stable solid spheres can be

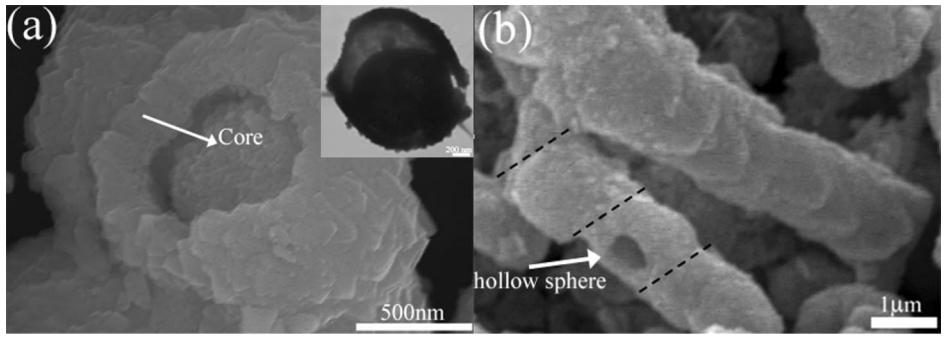

Figure 9. SEM and TEM (inset) images of the as-prepared (a) sphere-in-sphere structure and (b) bead-like tubular structure.

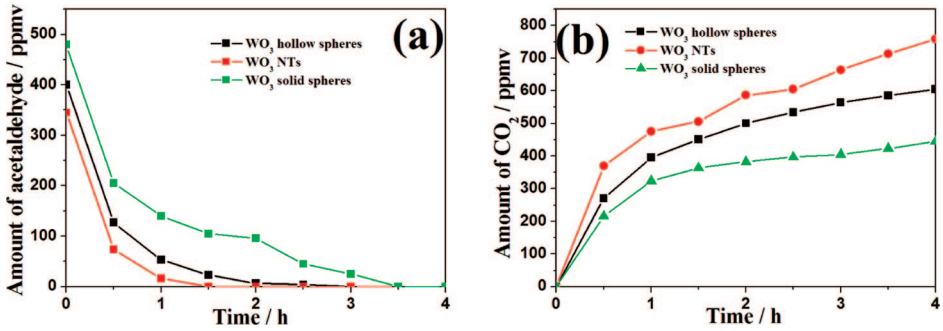

Figure 10. Plots of (a) the decrease in the acetaldehyde concentration and (b) the increase in the CO_2 concentration versus irradiation time during photocatalytic degradation of about 500 ppmv acetaldehyde.

produced by the aggregation of massive nanoparticles in a short time due to the absence of the dissolution−reprecipitation effect because the driving force for precipitation is very large at a large OH^- concentration. Thus, an optimum urea amount for the synthesis of hollow structures is necessary in this WCl_6/urea/ethanol system.

Photocatalytic Activity. Tungsten oxide was once considered to be inactive for oxidation of organic contaminants in air because of its low conduction band level and low reduction power of electrons to reduce absorbed oxygen molecules. Recently, several groups have reported efficient cocatalysts with WO_3 such as Pt,[29−31] Pd,[32] tungsten carbide (WC),[33] the Cu(II) ion,[34] and CuO,[35] which enhance the visible light activity of WO_3 by the multielectron reduction process. On the other hand, the activities of semiconductor photocatalysts largely depend on physical and chemical properties, especially crystallinity and surface area.[30] Nanostructured photocatalysts with controlled morphologies and microstructures usually exhibit enhanced photocatalytic activities due to large surface areas and novel structures. A previous study on the shape-controlled synthesis has already confirmed that the relationship between morphology and photocatalytic activities of these nanomaterials did exist.[20] Here, the photocatalytic activity of the obtained WO_3 powders with different morphologies in our experiment was evaluated by measuring the decrease in acetaldehyde and the production of CO_2 in the gas phase upon visible light irradiation. In our previous study, WO_3 nanotubes show a higher photocatalytic activity after Pt loading for the degradation of gas-phase acetaldehyde than that of commercial WO_3 particles and nitrogen-doped TiO_2.[22] Figure 10 shows a comparison of the photocatalytic activity of WO_3 nanotubes, hollow spheres, and solid spheres after 0.5 wt % Pt loading. It is clear that the photocatalytic activity of WO_3 nanotubes was better than that of WO_3 hollow spheres and also was superior to that of WO_3 solid spheres. The different BET surface area and optical adsorption were likely responsible for the behavior. Because the surface area of WO_3 nanotubes (25.0 m^2g^{-1}) and hollow spheres (24.0 m^2g^{-1}) was larger than that of solid spheres (13.4 m^2g^{-1}), nanotubes and hollow spheres showed higher photocatalytic activities than solid spheres. Optical absorption also strongly interrelates with the microstructures and morphologies of photocatalysts. The incident photons may be more effectively absorbed in nanotubes than in hollow spheres because the tubular structures are more favorable for light scattering, which results in the nanotubes showing higher activity.[36]

Conclusion

In summary, we presented the shape evolution of tungstic acid hollow structures from hollow spheres and hollow boxes to nanotubes by a nonaqueous and surfactant-free solvothermal method. This method is based on a mild and direct reaction between WCl_6 and urea in an ethanol solution. A variety of experimental factors such as the urea amount, ethanol amount, reaction time, temperature, and pH value were shown to play important roles in the formation of the hollow structures with different morphologies. On the basis of the results of the control experiments, we put forward a mechanism for the formation of hollow structures. After slow annealing, WO_3 hollow structures with porosity on the wall were obtained. Upon Pt loading, WO_3 nanotubes showed a higher photocatalytic activity for the degradation of gas-phase acetaldehyde than did hollow spheres and solid spheres. These nanoporous-walled WO_3 hollow structures are expected to find promising applications in catalysis and electrochemistry and as templates and supporting hosts for other materials.

Acknowledgment. This work was supported by the New Energy and Industrial Technology Development Organization (NEDO). This work was partly conducted in the AIST Nano-Processing Facility, which was supported by the Nanotechnology Support Project of the Ministry of Education, Culture, Sports, Science, and Technology of Japan.

References and Notes

(1) Wang, Y. H.; Chen, P. L.; Liu, M. H. *Nanotechnology* **2008**, *19*, 045607.

(2) Fei, J. B.; Cui, Y.; Yan, X. H.; Qi, W.; Yang, Y.; Wang, K.; He, Q.; Li, J. B. *Adv. Mater.* **2008**, *20*, 452.

(3) Xie, L.; Zheng, J.; Liu, Y.; Li, Y.; Li, X. G. *Chem. Mater.* **2008**, *20*, 282.

(4) Liang, H. P.; Lawrence, N. S.; Wan, L. J.; Jiang, L.; Song, W. G.; Jones, J. T. *J. Phys. Chem. C* **2008**, *112*, 338.

(5) Lou, X. W.; Archer, L. A.; Yang, Z. C. *Adv. Mater.* **2008**, *20*, 3987.

(6) Chen, G. C.; Kuo, C. Y.; Lu, S. Y. *J. Am. Ceram. Soc.* **2005**, *88*, 277.

(7) Martinez, C. J.; Hockey, B.; Montgomery, C. B.; Semancik, S. *Langmuir* **2005**, *21*, 7937.

(8) Caruso, F.; Spasova, M.; Susha, A.; Giersig, M.; Caruso, M. *Chem. Mater.* **2001**, *13*, 109.

(9) Zhang, H.; Zhang, S. Y.; Pan, S.; Li, G. P.; Hou, J. G. *Nanotechnology* **2004**, *15*, 945.

(10) Liang, H. P.; Zhang, H. M.; Hu, J. S.; Guo, Y. G.; Wang, L. J.; Bai, L. *Angew. Chem., Int. Ed.* **2004**, *43*, 1540.

(11) He, T.; Yao, J. N. *J. Mater. Chem.* **2007**, *17*, 4547.

(12) Choi, H. G.; Jung, Y. H.; Kim, D. K. *J. Am. Ceram. Soc.* **2005**, *88*, 1684.

(13) Lou, X. W.; Zeng, H. C. *Inorg. Chem.* **2003**, *42*, 6169.

(14) Lee, K.; Seo, W. S.; Park, J. T. *J. Am. Chem. Soc.* **2003**, *125*, 3408.

(15) Gu, Z.; Ma, Y.; Yang, W.; Zhang, G.; Yao, J. *Chem. Commun.* **2005**, 3597.

(16) Polleux, J.; Pinna, N.; Antonietti, M.; Niederberger, M. *J. Am. Chem. Soc.* **2005**, *127*, 15595.

(17) Liu, Z. W.; Bando, Y.; Tang, C. C. *Chem. Phys. Lett.* **2003**, *372*, 179.

(18) Polleux, J.; Gurlo, A.; Barsan, N.; Weimar, U.; Antonietti, M.; Niederberger, M. *Angew. Chem., Int. Ed.* **2006**, *45*, 261.

(19) Li, X. L.; Lou, T. J.; Sun, X. M.; Li, Y. D. *Inorg. Chem.* **2004**, *43*, 5442.

(20) Chen, D.; Ye, J. H. *Adv. Funct. Mater.* **2008**, *18*, 1922.

(21) Pinna, N.; Niederberger, M. *Angew. Chem., Int. Ed.* **2008**, *47*, 5292.

(22) Zhao, Z. G.; Miyauchi, M. *Angew. Chem., Int. Ed.* **2008**, *47*, 7051.

(23) Barrett, E. P.; Joyner, L. G.; Halenda, P. P. *J. Am. Chem. Soc.* **1951**, *73*, 373.

(24) Lou, X. W.; Wang, Y.; Yuan, C. L.; Lee, Y.; Archer, A. L. *Adv. Mater.* **2006**, *18*, 2325.

(25) Caputo, G.; Adami, R.; Reverchon, E. *Cryst. Growth Des* **2008**, *8*, 2707.

(26) Wang, Y. W.; Zhang, L. Z.; Deng, K. J.; Chen, X. Y.; Zou, Z. G. *J. Phys. Chem. C.* **2007**, *111*, 2709.

(27) Custelcean, R. *Chem. Commun.* **2008**, 295.

(28) Li, M. X.; Bian, Z. F.; Zhu, J.; Zhang, D. Q.; Li, G. S.; Huo, Y. N.; Li, H.; Lu, Y. F. *J. Am. Chem. Soc.* **2007**, *129*, 8406.

(29) Abe, R.; Takami, H.; Murakami, N.; Ohtani, B. *J. Am. Chem. Soc.* **2008**, *130*, 7780.

(30) Sadakane, M.; Sasaki, K.; Kunioku, H.; Ohtani, B.; Ueda, W.; Abe, R. *Chem. Commun.* **2008**, 6552.

(31) Miyauchi, M. *Phys. Chem. Chem. Phys.* **2008**, *10*, 6258.

(32) Arai, T.; Horiguchi, M.; Yanagida, M.; Gunji, T.; Sugihara, H.; Sayama, K. *Chem. Commun.* **2008**, 5565.

(33) Kim, Y. H.; Irie, H.; Hashimoto, K. *Appl. Phys. Lett.* **2008**, *92*, 182107.

(34) Irie, H.; Miura, S.; Kamiya, K.; Hashimoto, K. *Chem. Phys. Lett.* **2008**, *457*, 202.

(35) Arai, T.; Yanagida, M.; Konishi, Y.; Iwasaki, Y.; Sugihara, H.; Sayama, K. *Catal. Commun.* **2008**, *9*, 1254.

(36) Mor, G. K.; Shankar, K.; Paulose, M.; Varghese, O. K.; Grimes, C. A. *Nano Lett* **2005**, *5*, 191.

JP900160U